PARAMETER ESTIMATION OF SOCIAL FORCES IN PEDESTRIAN DYNAMICS MODELS VIA A PROBABILISTIC METHOD

Alessandro Corbetta

CASA- Centre for Analysis, Scientific computing and Applications
Department of Mathematics and Computer Science
Eindhoven University of Technology
P.O. Box 513, 5600 MB Eindhoven, The Netherlands
and
Department of Structural, Geotechnical and Building Engineering
Politecnico di Torino, Corso Duca degli Abruzzi 24, 10126 Torino, Italy

Adrian Muntean

CASA- Centre for Analysis, Scientific computing and Applications
ICMS - Institute for Complex Molecular Systems
Department of Mathematics and Computer Science
Eindhoven University of Technology
P.O. Box 513, 5600 MB Eindhoven, The Netherlands

Kiamars Vafayi

CASA- Centre for Analysis, Scientific computing and Applications
Department of Mathematics and Computer Science
Eindhoven University of Technology
P.O. Box 513, 5600 MB Eindhoven, The Netherlands
(corresponding author)

Abstract. Focusing on a specific crowd dynamics situation, including real life experiments and measurements, our paper targets a twofold aim: (1) we present a Bayesian probabilistic method to estimate the value and the uncertainty (in the form of a probability density function) of parameters in crowd dynamic models from the experimental data; and (2) we introduce a fitness measure for the models to classify a couple of model structures (forces) according to their fitness to the experimental data, preparing the stage for a more general model-selection and validation strategy inspired by probabilistic data analysis. Finally, we review the essential aspects of our experimental setup and measurement technique.

1. Introduction.

1.1. **Background.** Crowd models are powerful tools to explore the complex dynamics which characterizes the motion of pedestrians, cf. e.g. the overview [29] and references cited therein. Understanding how crowds move and eventually being able to predict their behavior under given (possibly extreme) conditions becomes an increasingly important matter for our society. Reliable mathematical models

---

for crowds would be of great benefit, for instance, to increase pedestrian comfort (ensuring a regular flow motion at acceptable densities), security (evacuation assessments) and structural serviceability (crowd-structure interaction), in particular if the theoretical information/forecast is in real-time agreement with the actual crowd behavior.

Aiming at quantitative models, a proper assessment of the uncertainty is needed given experimental data (e.g., in the form of crowd recordings) together with a model or a collection of models. This paper treats a basic crowd scenario: pedestrians crossing an U-shaped landing (corridor) in a defined direction. In particular, the questions we consider here relate to a low density regime, in which pedestrians can be considered as moving alone, being just influenced by their desires as well as the geometry of the (built) environment in their surroundings ("rarefied gas" regime). We explicitly wonder (in a quantitative sense specified afterwards): do pedestrians *interact* with walls? How does the presence of walls affect the pedestrian motion? Are walls purely repulsive, or could they be attractive?

To address these (and related) questions, extensive video recordings of a trafficked U-shaped landing in Eindhoven University of Technology (see Appendix A) have been made and 7 different test models describing the pedestrian-wall interaction are deducted and compared against.

1.2. **Simple crowd models. Ensembles.** Since the movement of pedestrians is to a large extent non-deterministic, any model that describes the detailed motion of pedestrians requires the introduction of some elements of noise. To address this issue, one may choose to describe the dynamics from a "coarse grained" point of view, hence either at the mesoscopic scale or at the macroscopic scale. For instance, when a macroscopic level of description is used, a balance equation for the density of pedestrians (possibly supported by balance of momentum, see e.g. [9] for details on balance laws) models the evolution of the crowd, while the detailed microscopic behaviors are averaged out. In principle, the latter equations can be derived directly from the microscopic equations, although a problem remains: microscopic models for crowd dynamics (see, for instance, the social force model proposed by Helbing and Molnar [16]) describe the detailed motion of pedestrians, but to which extent the microscopic details are relevant to capture the intrinsic crowd patterns at larger scales and what is the role of noise and uncertainty? In other words, which details of the microscopic information are necessary to capture the behavior of the crowd?

Usually, in an attempt to keep into account the observed non-deterministic behavior of the crowds, noise is added to deterministic models turning them into Langevin-like equations for the so-called active Brownian particles (see e.g. [27, 29]) or in measure-valued evolutions (see e.g. [1, 14, 2]).

Since we cannot describe deterministically the motion of pedestrians, we opt for a different strategy. We choose to construct a probabilistic ensemble of pedestrians (referred here as the *ensemble*[1]) whose properties can be directly deduced in a quantitative manner on the basis of experimental observations.

We construct such crowd ensemble by the means of a connection to simple evolution models, which can be cast in the form of a potential of interaction of pedestrians with obstacles or amongst themselves together via Newtonian dynamics. The potential or force in the model is characterized by a set of parameters, whose statistical

---

[1]By "ensemble" we understand a collection of the copies of a system distributed according to a probability distribution function (pdf).

properties can be obtained by comparing the model with well-controlled experimental data. Thus the model and the probability distribution of the model parameters (inferred from data) define our *crowd ensemble*. In this way we cast *the force estimation problem* into a well defined procedure of probabilistic data analysis, very much inspired by [32, 31]. A related approach for traffic-flow models is mentioned in [17] and references therein.

1.3. **Aim of the paper.** We focus our attention on the effects of walls (obstacles) on pedestrian motion for a specific crowd dynamics scenario (extensively described in Section 1.4 from a qualitative point of view, and in the Appendix A from a technical point of view). Once the effect of walls is understood, considering pedestrian-pedestrian interactions in the same scenario is expected to be easier.

Note that even standard crowd dynamics situations are actually rather complex, in particular, the following aspects among others need to be considered carefully:

(i) the motion of pedestrian is complex and influenced by many sources, among others: desires/aims, interaction with geometry and interaction with neighboring peers;

(ii) the effects of these interaction appears simultaneously and in an entangled way.

To attempt to disclose the cause-effect relations in this complex motion, we choose a step by step approach; therefore, we opt to look exclusively at situations in which the interaction among pedestrians is absent and the motion is fully regulated by own desires and neighboring geometry. As a clear consequence, this study sets a possible stage for the analysis of pedestrian-pedestrian interactions which is inevitably perturbed by the effects mentioned at (i) and (ii). To make the complete dynamics approachable, the hypothesis of linear superposition of effects has to be made.

In social-force models [16, 11, 26, 34, 4] (for overviews on the matter see, e.g., [13, 29]), pedestrians move according to a Newtonian dynamics; in particular, in the absence of neighboring peers, the force acting on a single particle can be expressed as:

$$F = F_{v_d} + F_{wall}, \tag{1}$$

where

- F_{v_d} is a force which keeps into account the desires of the pedestrians in terms of the direction he/she is willing to follow. Usually, this term induces a relaxation of the velocity v of the pedestrian towards a background *desired velocity* field $v_d = v_d(x, y)$. The desired velocity field usually drives the pedestrian all over the domain toward a given "desired" target. In formulas, this term reads as $F_{v_d} = (v - v_d)/\tau$, where τ is a characteristic relaxation time.
- F_{wall} describes the interactions pedestrians have with walls. This term doesn't just model the impenetrability of the latter, rather it is aimed at taking into account the will of pedestrians to maintain a certain distance from walls.

Structure and parameters dependence of v_d and F_{wall} shall be assumed. In the following, we suppose v_d to be parametrized by its magnitude (the *desired speed* $|v_d| \equiv const$), whilst its direction is kept as a model feature.

On the other hand, F_{wall} is assumed to be a sum of forces pointing outwards the walls in the proximity of the particle, i.e.
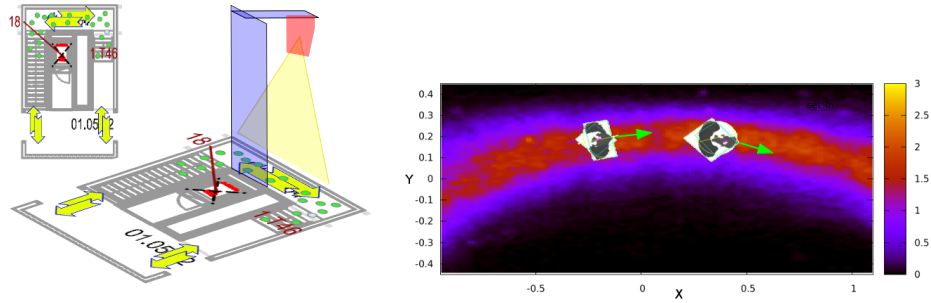
$$F_{wall} = \sum_{w \in W} F_{wall}^w,$$

FIGURE 1. Left: Representation of the landing map. Right: Actual view from the camera. Here two pedestrians are detected as they walk through the landing. Multi-pedestrian events, such as the one shown here for illustration, are actually filtered out, so that only trajectories involving only one pedestrian at a time are considered. The density plot in the background shows the density count of pedestrian, as measured from our camera and distributed over the 2D space of the landing, after a long time.

where the sum is performed on every wall w in the set of the walls W. One usually supposes that every contribution F_{wall}^w has a fixed functional form which depends on the distance between the pedestrian and the wall, and is parametrized by a set of N_p parameters $\vec{P} = \{P_1, P_2, \ldots, P_{N_p}\} = \{P_i\}$. Note, however, that different, more general, forms of F_{wall} can be chosen; see e.g. [18].

In the present work, our main purpose is to estimate the probability distribution functions of the model parameters v_d and $\{P_i\}$ from experimental data (cf. Section 1.4 and Appendix A).

1.4. **Experimental data.** The kinematic data referring to trajectories of pedestrians (positions, velocities, accelerations) walking through a rectangular section of a U-shaped landing (see Figure 1 and consider Appendix A for technical details) is acquired via an over head recording camera. In general, the landing features a rich pedestrian dynamics for its size; pedestrian walking in the two directions (in general, ascending and descending the stairs) can be continuously observed during working hours, and up to six pedestrians have been seen walking together at the same time.

Due to the geometry of the setting, trajectories of pedestrians tend to bend slightly as the landing is crossed. This is a consequence of the presence of 90 degree turns at the ends of the landing.

An more extensive description of the various dynamics recorded in the corridor, possibly conditioned to the direction and to the flow condition, can be found in the work [5] by the same authors.

In the following, since we focus our attention on the walls-pedestrian interaction, we consider only data concerning a single pedestrian (i.e. appearing alone in the camera field of view) and that has a specific desired direction (from the left to the right hand side of the landing). In other words, all recordings referring to situations in which more than one pedestrian is present at a time, or in which she is not going to the right, are not taken into consideration.

The measured data considered consists of a set T_s of N_{T_s} pedestrian trajectories, where $N_{T_s} \approx 1500$, i.e.

$$T_s = \{T_i | \, 1 \leq i \leq N_{T_s}\} \, .$$

Such large set of trajectory is assumed to give a complete, "statistically resolved", description of the considered behavior. In other words, it is assumed that enlarging the set T_s with further trajectories would not change its features significantly.

Every trajectory is itself a set of recorded points in the $(2+1)$-dimensional space-time of the landing; in other words, given a pedestrian having trajectory T_i, she assumes spatial position (x_k^i, y_k^i) at time instant t_k, where k is an integer ranging from 1 to the number of steps M_i describing the trajectory. In formulas, a trajectory can be therefore written as

$$T_i = \{(x_k^i, y_k^i, t_k^i) | \, 1 \leq k \leq M_i\}. \tag{2}$$

Remark 1. Looking back at the considered model parameters (i.e., the desired speed $|v_d|$ and the wall force parameters, $\{P_i\}$), we observe that $|v_d|$ is a parameter specific of the trajectories, i.e. to every trajectory it corresponds a specific value $|v_d|$ that needs to be estimated. In contrast, one can think of $\{P_i\}$ as a set of global parameters, in the sense that they are shared between all trajectories. This would suggest the use of a two-steps optimization procedure; see Section 2.4. In this paper, we decide to treat all parameters in the same way, and thus we postpone the two-steps optimization idea for a later approach.

1.5. **Structure of the paper.** The paper is organized as follows: Section 2 contains the working methodology which is based on probability estimates guided by Bayes theorem; moreover, how Bayes theorem can be used for model selection is pointed out. The main result of this paper is presented in Section 3: following the described working methodology, parameters of a number of simple wall force models for our crowd scenario are estimated. Furthermore, on this basis, models are compared quantitatively and qualitatively. Section 4 discusses the obtained results. Finally, the measurement technique and the collected experimental data are described in Appendix A.

2. **Probabilistic data analysis of crowd ensembles.** In this section, we introduce the methodology behind the probabilistic data analysis used here. For more details, we refer the reader to the introductory guide by Skilling [32] or to the mathematical background presented by Sivia in [31].

2.1. **Probability estimates. Bayes theorem.** We denote all the measured data by D and all prior information by I. In other words, while D encloses all the information acquired in the measurement process, I includes the assumptions made on model and thus on the type of dynamics.

Our goal is to identify the parameters for a considered set of pedestrian models $(|v_d|, \{P_i\})$ for the considered scenario. This task can be performed by estimating the *posterior* probability law

$$Prob\left(v_d, \{P_i\} \, | D, I\right),$$

which describes the probability associated to the parameters of a considered model being conditioned on data D and all prior information I. Such probability law can be either peaked around a given maximum value, which does correspond to the solution of the estimation problem, or can be dispersed. In such case the mean

value and the standard deviation of the law can be used as a fair representation of the full distribution.

By means of Bayes theorem (see e.g. [8, 7, 21]), the posterior probability can be related to other probabilities of easier computation (or even known already). The theorem reads as

$$Prob\left(v_d, \{P_i\} \,|D, I\right) = \frac{Prob\left(D|v_d, \{P_i\}, I\right) Prob\left(v_d, \{P_i\} \,|I\right)}{Prob\left(D|I\right)}. \qquad (3)$$

The probabilities involved in the l.h.s of Equation (3) are respectively

- the *likelihood function* $Prob\left(D|v_d, \{P_i\}, I\right)$;
- the *prior probability* $Prob\left(v_d, \{P_i\} \,|I\right)$;
- the *data evidence* $Prob\left(D|I\right)$.

In the following subsections such probabilities are extensively used and details regarding their computations are given. It is worth to notice that, since the data D is assumed as given, the data evidence plays the role of a mere normalization constant and, as a consequence, we can write

$$Prob\left(v_d, \{P_i\} \,|D, I\right) \approx Prob\left(D|v_d, \{P_i\}, I\right) Prob\left(v_d, \{P_i\} \,|I\right), \qquad (4)$$

to stress the fact that the quantities playing a significant role in parameter estimation are just the likelihood function and the prior probability.

2.2. **Likelihood function. Misfit norm(s).** The likelihood function measures how well the model, along with the given parameters, fits the data. We distinguish between four different schemes to compare data and models:

(i) positions in trajectory data versus positions predicted in the model;
(ii) velocities obtained from data versus velocities as calculated from the model;
(iii) acceleration deducted from data versus acceleration in the model;
(iv) a combination of the previous three.

It is worth to remark that the third scheme has the advantage of not requiring the computation of the full trajectories generated by the model. On the other hand, acceleration data are usually more noisy, as a consequence of the double time differentiation of pedestrian trajectories - which is itself never exempt from noise (see also [28] for further insights on acceleration-based comparison between models and data in the case of noisy measurements).

The likelihood function can be obtained from the Principle of Maximum Entropy (MaxEnt) once the kind of noise in the data is assumed, see [31] for details. In particular, assuming Gaussian noise, the likelihood function results in

$$Prob\left(D|v_d, \{P_i\}, I\right) = \Pi_{k=1}^{N_k} \left(\sigma_k \sqrt{2\pi}\right)^{-1} \exp\left(\frac{-\sum_{k=1}^{N_k} (d_k - m_k)^2}{2\sigma_k^2}\right), \qquad (5)$$

where d_k is the acceleration in the trajectory data, at sample k, and m_k is the acceleration provided by the model with parameters $|v_d|$ and $\{P_i\}$ at the same point. According to the adopted notation, σ_k is the error estimation, or standard deviation, for the experimental acceleration d_k.

In the following subsections, we consider the likelihood function for two different assumptions on the noise in the data: Gaussian noise (in 2.2.1) and Exponential noise (in 2.2.2). Further assumptions on the noise[2] may be made These two options seem to be more common in literature.

---

[2] Note that in the Bayesian framework the noise is part of the model.

For what concerns the analysis of real data reported in Section 3, the comparison between model and data is performed considering accelerations (scheme (iii)) and the noise is assumed to be Gaussian. The analysis of the actual noise structure is left for further investigations (see [6]).

2.2.1. *Gaussian noise.* The misfit function χ^2 is defined such that

$$\chi^2 = -2 \log Prob\left(D|v_d, \{P_i\}, I\right) + C(\sigma_k, N_k)$$

or

$$Prob\left(D|v_d, \{P_i\}, I\right) \approx \exp\left(\frac{-\chi^2}{2}\right).$$

Therefore, for the case of Gaussian noise in the data, we have the ℓ_2 norm for the "distance" between the model and data;

$$\chi^2 = \frac{\sum_{k=1}^{N_k}(d_k - m_k)^2}{\sigma_k^2}.$$

Since the logarithm is a monotonically increasing function, finding the maximum of $Prob\left(D|v_d, \{P_i\}, I\right)$ is equivalent to finding a minimum for χ^2. It becomes more simplified if σ_k are equal to σ,

$$\chi^2 = \frac{1}{\sigma^2} \sum_{k=1}^{N_k}(d_k - m_k)^2$$

or more reasonably since we would intuitively expect that the error estimate be proportional to the data $\sigma_k = \sigma |d_k|$ and define a new misfit norm by dividing the previous one by N_k;

$$\chi^2 = \frac{1}{N_k \sigma^2} \sum_{k=1}^{N_k}\left(\frac{d_k - m_k}{d_k}\right)^2.$$

Remark 2. Since we do not study explicitly the absolute magnitude of the noise, we take everywhere in the paper σ to be 1.

This form of χ^2 has the interesting property that if $m_k = d_k(1 + \epsilon\sigma)$, i.e., if the model misses the data by a (small) fraction of ϵ of the error estimate, then we have

$$\chi^2(\epsilon) = \epsilon^2.$$

2.2.2. *Exponential noise.* The exponential noise in the data corresponds to

$$Prob\left(D|v_d, \{P_i\}, I\right) = \Pi_{k=1}^{N_k}(2\sigma_k)^{-1} \exp\left(-\sum_{k=1}^{N_k}\frac{|d_k - m_k|}{\sigma_k}\right),$$

therefore the misfit χ^2 in this case will be the l_1 norm

$$\chi^2 = \sum_{k=1}^{N_k}\frac{|d_k - m_k|}{\sigma_k}.$$

Again if we assume $\sigma_k = \sigma |d_k|$ and divide by N_k we obtain

$$\chi^2 = \frac{1}{N_k \sigma} \sum_{k=1}^{N_k}\left|\frac{d_k - m_k}{d_k}\right|.$$

A similar calculation as the one we did for Gaussian noise for the deviation $m_k = d_k(1 + \epsilon\sigma)$, yields

$$\chi^2(\epsilon) = \epsilon.$$

The exponential distribution is less centrally distributed than a Gaussian. Consequently, the ℓ_1 norm is more robust and it is expected to fit better data that contains a number of "wildly" distributed points.

With our choice of the misfit functions χ^2, we are *de facto* pushing forward an empirical probability measure (defined by the data), from the parameter space onto the real line. This allows us to compare in a natural fashion different models.

2.3. **Prior probability.**

2.3.1. *Background.* The prior probability $Prob\,(v_d, \{P_i\}\,|\,I)$ encodes our prior state of knowledge on the parameters, before taking into account the acquired data D. For most practical purposes we can suppose that it is a constant over the range of parameters that we consider acceptable. More precisely we can use the symmetry group transformations and/or the principle of maximum entropy to assign the prior probabilities. From translation symmetry arguments, it turns out that for position parameters, like coordinates, a uniform prior distribution over the expected range is the optimal choice. For scale parameters, the right prior is the Jeffreys distribution $Prob\,(p) \propto \frac{1}{p}$, which is a consequence of scale invariance symmetry [21, 19, 20]. As long as the data is of good quality and the range of parameters is chosen well, one expects that the effect of the likelihood function dominates, and the posterior probability is less sensitive to the exact choice of the prior probability.

2.3.2. *Law of large numbers.* Since the number of trajectories measured can be arbitrarily large, we expect that the law of large numbers applies and that one can use an optimization procedure on each single trajectories separately and then employ the resulting histogram to estimated the parameters as the probability distribution for the value of the parameters. Thus having access to a large number of trajectories simplifies the estimation scheme.

2.4. **Two-steps optimization.**
As mentioned in Remark 1, the experimental technique and setup indicate that there is an intrinsic difference between the parameters v_d and $\{P_i\}$, the former being trajectory dependent and the later being global. One way to take this into account is to estimate firstly the parameters for each trajectory, in particular v_d, obtaining $v_{d,i}$ As the second step, one can afterwards use the data $\{(T_i, v_{d,i})\,|\,1 \le i \le N_T\}$ for globally estimating $\{P_i\}$ and calculating the global fitness of the model to data. We do not follow this approach here, rather we treat all parameters equally.

2.5. **Simulated annealing.**
The parameter space is in general multidimensional, and posterior probability is likely to be multi-modal, where the probability maximums (or the minimum of the misfit norm) are generally not analytically solvable. Among other techniques, one can use the simulated annealing method [22] to tackle this problem; in analogy with thermodynamics, one supposes that the misfit norm is an energy function and uses the Metropolis Monte Carlo algorithm [24] to sample the points in parameter space according to the Boltzmann-Gibbs distribution at a given temperature, T:

$$Prob_T\,(v_d, \{P_i\}) \propto e^{\frac{-\chi^2}{T}}.$$

Clearly by setting $T = 1$ we get the same distribution as the desired likelihood probability. The basic idea of simulated annealing is to start with $T > 1$ and then reduce the temperature dynamically until $T = 1$. In this way, starting from a more "energetic" point, it is more likely to overcome the local minimum traps of the misfit

function, and reach the most significant parts around the global minimum. Afterwards we will continue the sampling with $T = 1$ to obtain the points in parameter space distributed according to the posterior. In order to achieve good convergence, it might be necessary to repeat the whole annealing procedure several times and by starting from different random initial points. The resulting distribution can be used to obtain the marginal probability distribution of for example v_d;

$$Prob\left(v_d\right) = \int Prob_{T=1}\left(v_d, \{P_i\}\right) \prod dP_i,$$

which can be directly plotted or used to calculate the average and the standard deviation for the parameter;

$$\overline{v_d} = \langle v_d \rangle = \int v_d \, Prob_{T=1}\left(v_d, \{P_i\}\right) \prod dP_i$$

$$\sigma_{v_d}^2 := \left\langle (v_d - \overline{v_d})^2 \right\rangle = \int v_d^2 \, Prob_T\left(v_d, \{P_i\}\right) \prod dP_i \, - \, \overline{v_d}^2.$$

In the framework of this paper, using many trajectories as data, we perform the per-trajectory optimization approach mentioned in Section 2.3.2 and we thus do not require the simulated annealing approach.

2.6. **Selection and hierarchy of models.**

2.6.1. *Background.* Suppose we have two models M_A and M_B. In such case, we can apply the Bayes theorem to obtain

$$Prob\left(M_A|D, I\right) = \frac{Prob\left(D|M_A, I\right) Prob\left(M_A|I\right)}{Prob\left(D|I\right)}$$

and, similarly for M_B. Therefore, we have

$$\frac{Prob\left(M_A|D, I\right)}{Prob\left(M_B|D, I\right)} = \frac{Prob\left(D|M_A, I\right) Prob\left(M_A|I\right)}{Prob\left(D|M_B, I\right) Prob\left(M_B|I\right)}.$$

In general, the two models will have different set of parameters, $\overrightarrow{P}_A$ and $\overrightarrow{P}_B$, respectively. We have for the data D and assuming model M_A that

$$Prob\left(D|M_A, I\right) = \int Prob\left(D|\overrightarrow{P}_A, M_A, I\right) Prob\left(\overrightarrow{P}_A|M_A, I\right) d\overrightarrow{P}_A,$$

hence

$$\frac{Prob\left(M_A|D, I\right)}{Prob\left(M_B|D, I\right)}$$

$$= \frac{Prob\left(M_A|I\right)}{Prob\left(M_B|I\right)} \times \frac{\int Prob\left(D|\overrightarrow{P}_A, M_A, I\right) Prob\left(\overrightarrow{P}_A|M_A, I\right) d\overrightarrow{P}_A}{\int Prob\left(D|\overrightarrow{P}_B, M_B, I\right) Prob\left(\overrightarrow{P}_B|M_B, I\right) d\overrightarrow{P}_B}.$$

$Prob\left(M|I\right)$ indicates our prior probability for the model M. The integrals over the likelihood function can be calculated with the same stochastic procedure as explained in the section for simulated annealing. We see now that the parameters priors $Prob\left(\overrightarrow{P}|M, I\right)$ play a role, therefore it is important to make sure they are assigned properly, especially when the two models are nearly identical. We take here $\frac{Prob(M_A|I)}{Prob(M_B|I)} = 1$ but, in principle, this ratio does not need to be one and it can therefore be used for the updating procedures provided previous information are available.
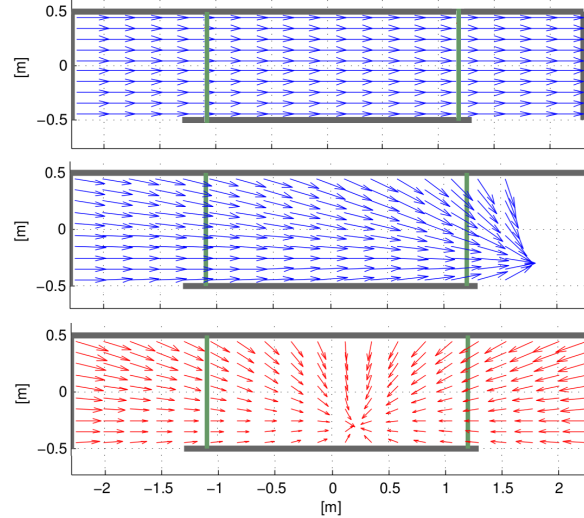
FIGURE 2. The setup of the models as seen from the camera. From up to bottom; the desired velocity field of M_1, the desired velocity field of M_3 and the force field of M_5.

2.6.2. *Law of large numbers.* As in the previous section, we use again the fact that we are in a law of large numbers regime and, after the optimization procedure on each single trajectory separately, we use the resulting histogram of the minimum value of the misfit function as the criteria for the model selection. If only one number is required to compare the models, it will be then the average of

$$L = \chi^2 \tag{6}$$

in such histograms, for each model, the smaller values are an indication that the model fits better to the data.

3. Estimating wall forces.

3.1. **Choice of models.** We consider 7 different *simple* crowd models which we denote by the symbols $M_1, M_2, \ldots, M_7$, respectively. We apply the probabilistic parameter estimation technique described in Section 2, together with our experimental test scenario described in Appendix A.

The chosen models aim at mimic the basic aspects of the pedestrian motion for individuals going from the left hand side to the right hand side of the landing as are observed in the experimental data. $M_1 - M_7$ feature different levels of complexity as more and more phenomenological aspects are introduced.

In the simplest case, a rightward directed homogeneous velocity field is considered as desired velocity and wall interaction is neglected (M_1, M_3). This basic hypothesis on the velocity is refined by considering a desired velocity field pointing toward an estimated exit point (M_2, M_4, M_7). Furthermore, as previously mentioned (see also Figure 1 (right)), pedestrian trajectories are slightly bending as a consequence of the landing shape. Turning pedestrians are *de facto* subjected to a (centripetal) force which we assume related to the presence of the walls. This observation defines the last refinement step for the models considered (M_5, M_6, M_7).

More precisely, the models $M_1 - M_7$ are:

M_1: An homogeneous desired velocity field parallel to the span-wise walls is adopted. The repulsion force of the walls is neglected. The relaxation time is hereby adopted as fixed and, according to [16], the value $\tau = 0.5s$ is chosen. As a consequence, the parameter to estimate is the desired speed $|v_d|$, i.e. $\overrightarrow{P}_1 = \{\}$; see Figure 2 (top).

M_2: An homogeneous velocity field analogous to the one in M_1 is chosen, however the relaxation time τ is also treated as a parameter to be estimated, i.e. $\overrightarrow{P}_2 = \{\tau\}$.

$M_{3,4}$: These models are similar - respectively - to M_1 and M_2, and they differ from the latter as the desired velocity field is such that at every point the desired velocity vector is directed towards the exit point, i.e. $\overrightarrow{P}_3 = \{\}$ and $\overrightarrow{P}_4 = \{\tau\}$; see Figure 2 (middle).

M_5: This model features exclusively the wall force F_{wall} and no relaxation toward a desired velocity field. In general, trajectories observed in the landing are slightly U-bending, hence a centripetal acceleration pointing toward the inner wall is expected. This is modeled via the wall force

$$F_{wall}(x,y) = m(x,y)\vec{\iota}(x,y),$$

where $m(x,y)$ is the magnitude of the force and $\vec{\iota}(x,y)$ is a unit vector field pointing toward an approximated acceleration center C, which, in this geometry, is close or lies on the lower wall. In the present case, C has been estimated from the tracks as the zero point of the average acceleration field as $C = (0.2, -0.3)m$. Generally speaking, for symmetry reasons, C can be expected to be approximately at the center of the lower wall (see Figure 2 (bottom)).

As this acceleration is expected to be mostly induced by the exterior walls, the magnitude $m(x,y)$ at a point (x,y) is modeled as

$$m(x,y) = A\sum_{i=1}^{3} e^{-kd(r_i(x,y))} + B,$$

where A, B and k are parameters to be estimated and $d(r_i(x,y))$ is the distance of the point (x,y) and the exterior walls (left, top, right: $i = 1, 2, 3$), i.e. $\overrightarrow{P}_5 = \{A, B, k\}$.

M_6: This is a particular case of M_5, where we suppose that the force magnitude is constant, i.e.

$$m(x,y) = A.$$

Here A is the parameter to be estimated, in other words, $\overrightarrow{P}_6 = \{A\}$.

M_7: This is similar to M_5, but, in addition to the force, a desired velocity is also taken into account. This desired velocity field is chosen to be similar to one in the models M_3 and M_4, pointing towards the exit. As in M_3, $\tau = 0.5s$, i.e. $\overrightarrow{P}_7 = \{A, B, k\}$.

3.2. **Optimization method.** We use the ℓ_2 norm for the misfit function (corresponding to the choice of Gaussian noise) and a "global" brute-force-based optimization procedure to find the best fitting parameters per trajectory. *A priori* knowledge on the parameters range is assumed; this defines a box β_* in the parameters space. The box is sampled by means of an orthogonal fine grid and the cost function is evaluated on every node. A gradient descent approach is then applied starting from the sample of minimum cost so to further refine the result.
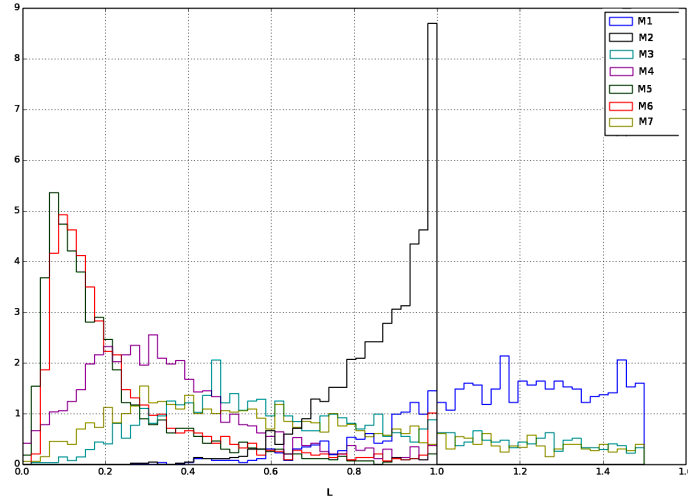
FIGURE 3. The empiric distribution of misfit (L) of the considered models is reported in these histograms (cf. Equation 6). The performances of a model in terms of accordance with the data are higher whenever the misfit is low - i.e. the misfit distribution is closer to zero. This happens in the cases of models M_5 and M_6.

The aforementioned *a priori* knowledge is built upon two criteria: whenever a parameter has clear physical interpretation (e.g. a desired speed $|v_d|$) then its limits are defined to be physically admissible (e.g. $0 \leq |v_d| \leq 2m/s$); otherwise, a decreasing sequence of coarse sampled "test" parameter boxes $\beta_0 \supset \beta_1 \supset \beta_2 \supset \ldots$ is used to estimate a feasible "final" parameter box β_* which is then analyzed with a finer grid. In other words, a "large", arbitrary, parameter box β_0 is considered first. Such box is then sampled with a coarse grid and the empiric distribution function of the optimal parameters is found. The box size is then reduced up to a box β_* in a way such that the support of the optimal parameter distribution lies entirely in it.

The behavior of the optimization method with respect to the choice of the model must finally be commented. The most relevant scaling factor for what concerns the computation time of the optimal model parameters is the dimension of the parameter space. In particular, when such a brute force algorithm is used, the computation time grows exponentially with the dimensions of the parameter space. In this context one can take full advantage of parallel computing as the duty of the search in the parameter space can be evenly split among different computing nodes.

In Figure 3, models can be compared on the basis of the empiric distribution (histogram) of the associated misfit functions. These empiric distributions provide insights on the capabilities of the model to be in accordance with the data. The closer the misfit distribution is to zero, the better the model behavior. Such empiric distributions have been obtained by the obtained optimal parameter distributions reported in Figures 4 and 5. Finally, in Table 1 the average values of the parameters and the misfit norms calculated from the histograms are reported.

3.3. **First observations.** Looking at the results of the estimation method shown in Figure 3 in terms of empiric distribution of misfit L, we observe that in the sense
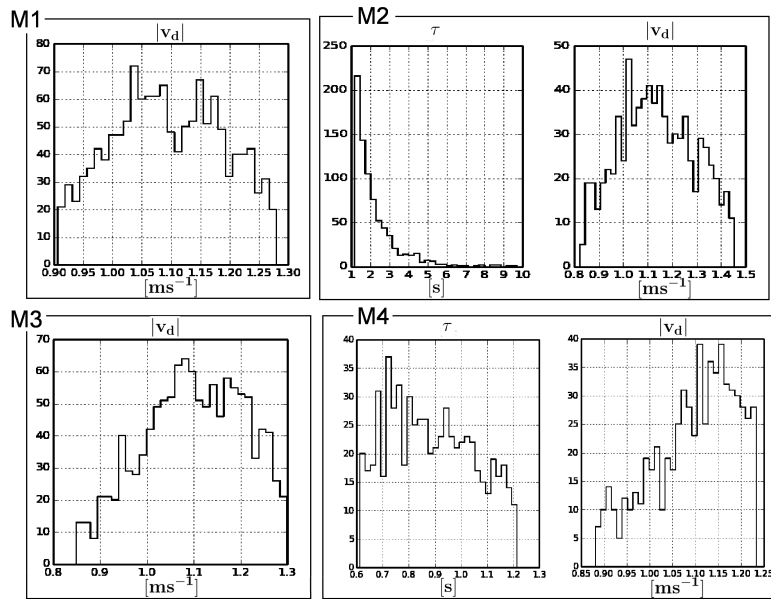
FIGURE 4. Histogram distributions (counts (frequency) *vs.* values) for the value of parameters corresponding to models $M_1, \ldots, M_4$.
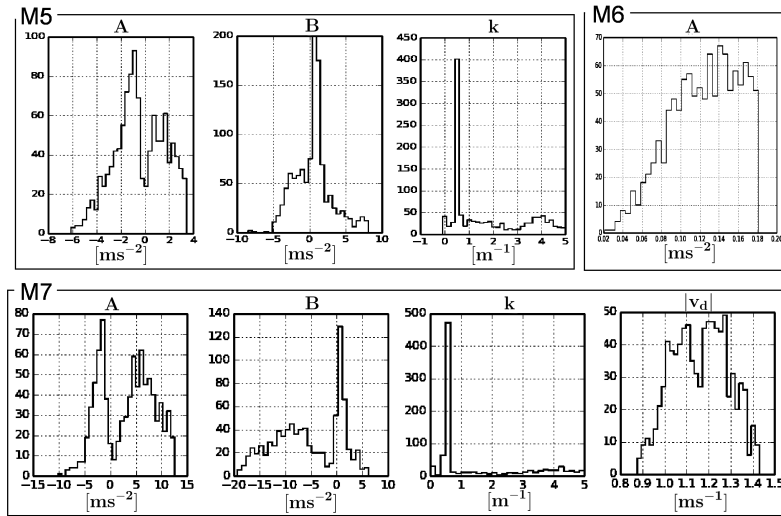

FIGURE 5. Histogram distributions (counts (frequency) *vs.* values) for the value of parameters corresponding to models $M_5, \ldots, M_7$.

of accordance with the data the two best performing models are the force-only models, i.e. M_5 and M_6; good performances are also provided by M_3.

We choose $\langle L \rangle$, i.e. the average value of L, as a synthetic comparison quantity (see also Table 3.3). The wide reduction of $\langle L \rangle$ in M_4 when compared to M_2 shows the importance of having a "good" desired velocity field and that more complicated

Model	$A[ms^{-2}]$	$B[ms^{-2}]$	$k[m^{-1}]$	$|v_d|[ms^{-1}]$	$\tau[s]$	$\langle L \rangle[1]$
M_1	-	-	-	1.11	-	1.30
M_2	-	-	-	1.18	2.14	0.83
M_3	-	-	-	1.13	-	0.81
M_4	-	-	-	1.20	1.40	0.33
M_5	-0.016	0.55	1.31	-	-	0.20
M_6	0.13	-	-	-	-	0.25
M_7	3.05	-3.85	1.02	1.19	-	0.73

TABLE 1. Average value of models parameters and the misfit norm

fields might possibly reduce $\langle L \rangle$ even further. However, the value of $\langle L \rangle$ in the case of M_4 is still larger than the value of $\langle L \rangle$ produced by M_5, which uses a quite simple force field.

Comparing the outcome in the case of models M_1 and M_2 (or similarly in the case of models M_3 and M_4), we notice that the introduction of the extra parameter for the relaxation time τ decreases $\langle L \rangle$, thus producing a better fit to the data. However doing that has a negligible effect on the magnitude of the desired velocity. The average τ, on the other hand, is rather dependent on the desired velocity field, as it can be seen from a comparison of models M_2 and M_4, but again the average magnitude of the desired velocity is not very sensitive to the choice of the field and in fact it varies negligibly across the models M_1, M_2, M_3, M_4 and M_7. The estimated desired speed shows agreeing values (see the histograms of $|v_d|$ in Figures 4 and 5, and its average values in Table 3.3) which, furthermore, are slightly overestimating the actual pedestrian velocities measured ($\langle v \rangle \approx 1.05 m/s$) consistent with the fact that they define a comfortable target velocity the pedestrians aim at achieving.

We found considerable correlations between the values of A and B in the models M_5 and M_7. This indicates that the data that we have is not able to estimate these two parameters separately very well, but their sum $A + B$ can be rather well estimated, which is approximately (given that k in M_5 and M_7 is small) what is being done in M_6, where the histogram for A is more sharply peaked than the histogram for either A or B in the models M_5 and M_7.

Finally, as firstly stated in Section 1.4, since a large set of experimental data (T_s) has been used, no significant difference in the statistical behavior of L is expected when adding more trajectories. In other words, we expect the "common" behavior adopted by single pedestrians when crossing the facility from left to right to be satisfactorily described by the sample of trajectories contained in T_s.

4. **Discussion.** Focusing on a specific pedestrian dynamics scenario, we presented a procedure for quantifying the fitness of pedestrian movement models and for estimating the related parameters. Such procedure has hence been used on measured, "real life", pedestrian trajectories. Basing the method on Bayesian foundations, we indicated how having access to a large number of measurements simplifies and improves the procedures of models selection and estimation of parameters.

When considering force-based pedestrian dynamics models, the force defined by the relaxation toward a desired velocity field and the "external" force acting on pedestrians due to walls are two different modeling routes and ingredients, used sometimes separately, and sometimes in combination. For instance, in the original social force model [16] both ingredients are present. In the simple landing setup
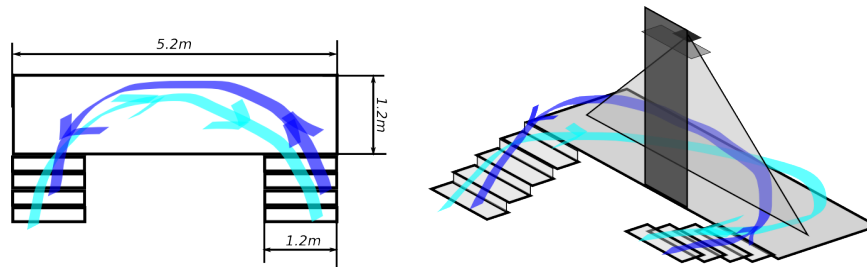
FIGURE 6. Schematics of the experimental site; on the left: top view; on the right: perspective view. The geometry of the staircases at the ends of the landing induces curved trajectories.

studied in this paper, both forces expressed through simple models have been considered. In particular, we found that the force-only models do a significantly better job in matching the data and apparently outperform also models that combine force and desired velocities. This is presumably due to the fact that the slight increased complexity of the model is not necessarily producing better fit to the data in general. The outcome of such increase in models complexity is nontrivial.

Possible extensions of this work can go in multiple directions: for instance, one definitely needs to study other geometries and flow conditions - this would allow the deduction of more abstract and transversal models to describe the interaction among pedestrians and walls. More detailed models allowing for instance the interplay between pedestrian(s)-wall vs. pedestrian-pedestrian interaction have to be considered as well, hence compared with the case of the single pedestrian preliminarily explored (at least in this scenario) hereby, e.g. as perturbations. Last but not least, we expect that from the experimental measurements much can be learned on the time and space structure of the correlations in the pedestrian flow (to be followed by us in [6]).

Finally, it is worth to note that the approach presented here is not exclusively meant for crowd dynamics applications. The parameter identification procedure can be exploited in a large variety of settings ranging from the tracking of cells motion in biological flows, the motion of colloidal suspensions, the detection of localization patterns of stress-driven defects in materials.

Appendix A. Experimental setup. We provide hereby fundamental information on the experimental setup and data used in this paper.

A.1. **Lagrangian measurement of pedestrian dynamics.** The experimental data considered in this paper, which have been used as a reference to tune and to compare pedestrian models, have been collected during a months-long experimental campaign.

A heavily trafficked landing (see Figure 6), which connects the canteen to the dining area of the MetaForum building at Eindhoven University of Technology, has been recorded on full-time (24/7) basis. These recordings allowed us to gather the statistics concerning pedestrian trajectories that we considered throughout this manuscript.

It is important to highlight that our data do not refer to pedestrians instructed *a priori* to cross the landing (as common in many "laboratory" crowd experiments); rather, they refer to the actual, unbiased, "field" measurement of pedestrian traffic.
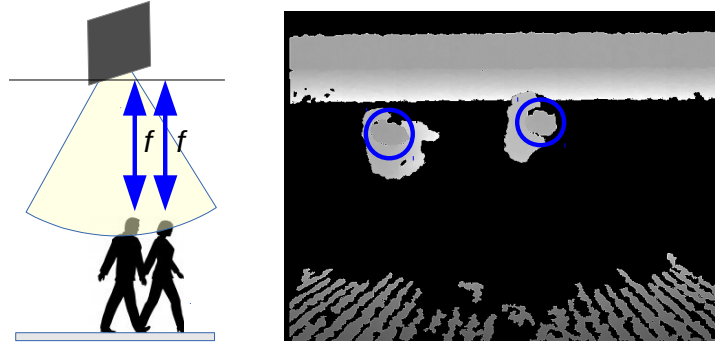
FIGURE 7. Left: schematic of how the sensor observe pedestrians passing in the landing; on the right: actual depth map recorded in the measurement site.

Following an approach similar to the one already introduced by Seer *et al.* [30], we performed recordings by employing a standard commercial *Kinect*$^{\mathrm{TM}}$ sensor by Microsoft Corp. [25] that allows reliable acquisition of pedestrian positions.

The Kinect$^{\mathrm{TM}}$ sensor is equipped with a special camera designed to enhance *natural interaction*, i.e. an interaction with computers and the gaming consoles (Microsoft Xbox 360$^{\mathrm{TM}}$) based on movements. In particular, in addition to an ordinary camera, the Kinect$^{\mathrm{TM}}$ is able to perform hardware measurements of the *depth map* of the observed scene. The depth map is a two dimensional grey-scale map which associates to every recorded pixel an intensity proportional to its distance from the camera plane (see Figure 7). In our experiments, in order to track pedestrians, we did not acquire any recordings from the standard camera, rather we relied totally on the depth map measurements.

As typically done in literature (cf. e.g. [15, 3, 23]) when one is concerned with the measurement of pedestrian trajectories, it is often favorable to record the top view of the scene. From the top view phenomena like partial body exposure to the camera or mutual hiding are absent. The problem of constructing pedestrian trajectories can be solved via identification and tracking of heads. Although the heads are always exposed to a top-viewing camera, performing their automatic tracking without additional hypothesis, e.g. on the clothing of pedestrian, can be hard. As pointed out in [30], the depth map associated to the top view of a given scene can be fruitfully used to detect heads. Heuristically speaking, the objects which are closest to the camera generate the local minima in the depth map: such objects, *modulo* a background subtraction, are *most likely* to be heads.

A.2. **The algorithm.** To generate pedestrian trajectories, "raw" depth maps are first processed to detect heads positions; then, a multi-particle tracking algorithm is used to estimate trajectories.

Specifically, the head detection procedure in use has been firstly introduced in [30], whilst well-established tracking algorithms in use in experimental fluid mechanics (and specifically in Particle Tracking Velocimetry (PTV)) have been used for the reconstruction of the trajectories.

For sake of completeness the whole algorithmic procedure is reported (steps 1,2,4,5,6 can be found in [30], Section 2.2, as steps 1,2,3,5).

Let $f^n = f^n(z)$ be the depth map recorded by Kinect$^{\text{TM}}$ (VGA resolution $640 \times 480px^2$) at time instant n and at position z, i.e.

$$f^n(z) := dist(\text{element in } z, \text{camera plane}), \tag{7}$$

where $z = (x, y)$ is a point in the VGA frame.

1. **Background subtraction.** In the recorded picture, and hence in the depth maps, a common background is expected.

   To detect pedestrians, the foreground must be first isolated. Let $B = B(z)$ be a depth map of the background (possibly built after suitable averages of empty backgrounds), the foreground $F^n = F^n(z)$ associated to a depth map $f^n = f^n(z)$ is obtained through the thresholding

   $$F^n(z) \leftarrow f^n(z) \cdot [f^n(z) - B(z) > \epsilon_1],$$

   where $\epsilon_1 > 0$ is a given (small) threshold, and $[P] = 1$ if proposition "P" holds true, $[P] = 0$, otherwise.

2. **Height thresholding.** A second thresholding operation is performed to eliminate objects which, although part of the foreground, are too small to be pedestrians, i.e.

   $$F^n(z) \leftarrow F^n(z) \cdot [F^n(z) > h_1].$$

3. **Foreground noise reduction** In dependence on the complexity of the filmed scene, $F^n(z)$ may present small, intermittent, misdetected spots. Such spots are removed by filtering out all the connected components of $F^n(x)$ (considering an 8-neighbor pixels based connection) whose area is smaller than a given threshold ϵ_2.

4. **Generation of a sparse depth map.** For computational reasons, the foreground of the thresholded depth map F^n is random sampled generating a *sparse* depth map of N samples

   $$F_s^n = \{(z_1, F^n(z_1)), (z_2, F^n(z_2)), \ldots, (z_N, F^n(z_N))\},$$

   where every pair $(z_i, F^n(z_i))$ satisfies $F^n(z_i) \neq 0$, i.e. the selected sample owns to the foreground and, *likely*, to a pedestrian.

5. **Sparse samples clusterization and pedestrian detection.** In order to identify and isolate pedestrians, sparse samples are agglomerated in *macro-samples* which are likely to be in correspondence with pedestrians themselves.

   The agglomeration is performed via a *hierarchical clustering* based on the geometrical distance between points, in particular, a *complete linkage clustering* algorithm is used [12]. Heuristically speaking, the sparse samples get agglomerated in a binary fashion forming larger and larger macro-samples. Ideally, macro-samples whose mutual distance is larger than the scale length of the human body S (e.g., average distance between the shoulders) do correspond to individuals.

   The iterative agglomeration procedure merges macro-samples on the basis of their distance starting from the closest pairs. In particular, given two macro-samples q_1 and q_2, the metric used satisfies

   $$\begin{cases} d^\infty(q_1, q_2) = \max_{(z_1 \in q_1, z_2 \in q_2)} d^\infty(z_1, z_2), \\ d^\infty(z_1, z_2) = d(z_1, z_2), \ \textit{if } z_1 \textit{ and } z_2 \textit{ are simple samples}, \end{cases}$$

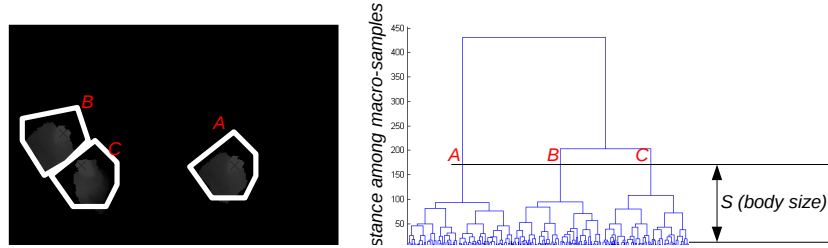   where d is the ordinary euclidean distance on the plane.

FIGURE 8. Left: depth map in which three pedestrians have been separated; on the right: cut dendrogram at height S, three macro-samples are present.

The procedure, which iteratively agglomerates all the points in just one super-sample, can be visualized via a dendrogram (see Figure 8).

To conclude, we observe that if the clusterization tree is truncated at an height S (having the same scale of the human body) than the mutual distances among all the sub-trees underneath that threshold provide estimates for the pedestrian in the scene.

6. **Head position estimation.** Given pedestrian identified by the cluster $C_j^n \in Q_m^n$, for some j, $1 \leq j \leq N^n$ (being N^n the total number of pedestrians present in frame n), we consider as head the set $H_j^n \subset C_j^n$ of samples whose depth is smaller than a given percentile α_k (usually $k = 10$) of the depth distribution of C_j^n,

$$H_j^n = \{z \in C_j^n \colon depth(z) \geq \alpha_k\}.$$

The head position is then estimated considering the centroid of the set, in formulas

$$\bar{z}_j^n = (x_j^n, y_j^n) = mean(H_j^n).$$

7. **Linking positions across the frames.** An estimate $\bar{z}_j^n$ of the heads position across the frames has been given. In order to approximate the pedestrian trajectories, heads positions must hence be tracked.

The problem of tracking time-sampled particle positions has been studied in several fields, in particular, it is central in Experimental Fluid Dynamics when a Lagrangian approach to flows is pursued. Following standard approaches in experimental Particle Tracking Velocimetry (PTV), and especially via OpenPTV [35, 33], Pedestrian trajectories are generated. In particular, sequences in the form of Equation (2) are obtained.

8. **Estimation of kinematic observables associated to trajectories.** Once the trajectories are known in their sampled form, kinematic observables such as velocities and accelerations must be estimated. Since the head estimation procedure is not exempt of measurement noise, and a certain degree of regularity in trajectories is expected, a smoothing spline (with smoothing parameter $\lambda = 1$) is used [10] (See Figure 9 for an example of some of the final trajectories).

After such procedure, the set of trajectories including relative velocities and accelerations is deduced.
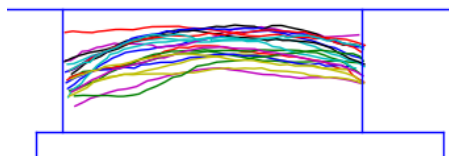
FIGURE 9. A sample selection of 20 pedestrian trajectories in the final data.

REFERENCES

[1] H. T. Banks and W. C. Thompson, *Least Squares Estimation of Probability Measures in the Prohorov Metric Framework*, Center for Research in Scientific Computation Tech Rep, CRSC-TR12-21, North Carolina State University, Raleigh, NC.

[2] N. Bellomo, B. Piccoli and A. Tosin, Modeling crowd dynamics from a complex system viewpoint, *Mathematical Models and Methods in Applied Sciences*, **22** (2012), 1230004, 29 pp.

[3] M. Boltes and A. Seyfried, Collecting pedestrian trajectories, *Neurocomputing*, **100** (2013), 127–133.

[4] L. Bruno and A. Corbetta, Multiscale probabilistic evaluation of the footbridge crowding. Part 2: Crossing pedestrian position, in *Proceedings of the 9th International Conference on Structural Dynamics, EURODYN 2014* (eds. A. Cunha, E. Caetano, P. Ribeiro and G. Müller), 2014, 937–944.

[5] A. Corbetta, L. Bruno, A. Muntean and F. Toschi, High statistics measurements of pedestrian dynamics, *Transportation Research Procedia*, **2** (2014), 96–104; The Conference on Pedestrian and Evacuation Dynamics 2014 (PED 2014), Delft, The Netherlands, October 2014, 22–24.

[6] A. Corbetta, A. Muntean, F. Toschi and K. Vafayi, Structural identification of interaction terms in a Langevin-like model for crowd dynamics, in preparation, 2014.

[7] R. T. Cox, Probability, frequency and reasonable expectation, *American Journal of Physics*, **14** (1946), 1–13.

[8] R. Cox, *Algebra of Probable Inference*, Algebra of Probable Inference, Johns Hopkins University Press, 1961.

[9] C. M. Dafermos, *Hyperbolic Conservation Laws in Continuum Physics*, Grundlehren der mathematischen Wissenschaften, Springer, Berlin, New York, 2000.

[10] C. De Boor, *A Practical Guide to Splines*, Vol. 27, Springer-Verlag, New York, 1978.

[11] P. Degond, C. Appert-Rolland, M. Moussaid, J. Pettre and G. Theraulaz, A hierarchy of heuristic-based models of crowd dynamics, *Journal of Statistical Physics*, **152** (2013), 1033–1068.

[12] R. O. Duda, P. E. Hart and D. G. Stork, *Pattern Classification*, John Wiley & Sons, 2012.

[13] D. C. Duives, W. Daamen and S. P. Hoogendoorn, State-of-the-art crowd motion simulation models, *Transportation Research Part C: Emerging Technologies*, **37** (2013), 193–209.

[14] J. Evers, S. C. Hille and A. Muntean, Well-posedness and approximation of a measure-valued mass evolution problem with flux boundary conditions, *Comptes Rendus Mathematique*, **352** (2014), 51–54.

[15] D. Helbing and A. Johansson, On the controversy around Daganzo's requiem for an Aw-Rascle's resurrection of second-order traffic flow models, *Modelling and Optimisation of Flows on Networks, Lecture Notes in Mathematics*, **2062** (2013), 271–302.

[16] D. Helbing and P. Molnar, Social force model for pedestrian dynamics, *Physical Review E*, **51** (1995), pp. 4282.

[17] S. Hoogendoorn and R. Hoogendoorn, Calibration of microscopic traffic-flow models using multiple data sources, *Philosophical Transactions of the Royal Society A: Mathematical, Physical and Engineering Sciences*, **368** (2010), 4497–4517.

[18] N. Jaklin, A. Cook and R. Geraerts, Real-time path planning in heterogeneous environments, *Computer Animation and Virtual Worlds*, **24** (2013), 285–295.

[19] E. T. Jaynes, Prior probabilities, *Systems Science and Cybernetics, IEEE Transactions on*, **4** (1968), 227–241.

[20] E. T. Jaynes, The well-posed problem, *Foundations of Physics*, **3** (1973), 477–492.

[21] E. T. Jaynes, *Probability Theory: the Logic of Science*, Cambridge University Press, 2003.

[22] S. Kirkpatrick and M. Vecchi et al., Optimization by simulated annealing, *Science*, **220** (1983), 671–680.

[23] X. Liu, W. Song and J. Zhang, Extraction and quantitative analysis of microscopic evacuation characteristics based on digital image processing, *Physica A: Statistical Mechanics and its Applications*, **388** (2009), 2717–2726.

[24] N. Metropolis, A. W. Rosenbluth, M. N. Rosenbluth, A. H. Teller and E. Teller, Equation of state calculations by fast computing machines, *Journal of Chemical Physics*, **21** (1953), 1087–1092.

[25] Microsoft Corp., *Kinect for Xbox 360*, Redmond, WA, USA.

[26] M. Moussaid, D. Helbing and G. Theraulaz, How simple rules determine pedestrian behavior and crowd disasters, *Proceedings of the National Academy of Sciences*, **108** (2011), 6884–6888.

[27] P. Romanczuk, M. Bär, W. Ebeling, B. Lindner and L. Schimansky-Geier, Active Brownian particles, *The European Physical Journal Special Topics*, **202** (2012), 1–162.

[28] C. Rudloff, T. Matyus and S. Seer, Comparison of different calibration techniques on simulated data, in *Pedestrian and Evacuation Dynamics 2012*, Springer International Publishing, 2014, 657–672.

[29] A. Schadschneider, D. Chowdhury and K. Nishinari, *Stochastic Transport in Complex Systems: From Molecules to Vehicles*, Elsevier, 2010.

[30] S. Seer, N. Brändle and C. Ratti, Kinects and human kinetics: A new approach for studying pedestrian behavior, *Transportation Research Part C: Emerging Technologies,* **48** (2014), 212–228.

[31] D. S. Sivia, *Data Analysis: A Bayesian Tutorial*, Oxford University Press, 1996.

[32] J. Skilling, Probabilistic data analysis: An introductory guide, *Journal of Microscopy*, **190** (1998), 28–36.

[33] The OpenPTV Consortium, OpenPTV: Open source particle tracking velocimetry, 2012.

[34] A. U. K. Wagoum, A. Seyfried and S. Holl, Modeling the dynamic route choice of pedestrians to assess the criticality of building evacuation, *Advances in Complex Systems*, **15** (2012), 1250029, 22 pp.

[35] J. Willneff, *A Spatio-Temporal Matching Algorithm for 3D Particle Tracking Velocimetry*, Mitteilungen-Institut für Geodäsie und Photogrammetrie an der Eidgenossischen Technischen Hochschule Zürich, 2003.

E-mail address: a.corbetta@tue.nl
E-mail address: a.muntean@tue.nl
E-mail address: k.vafayi@tue.nl